Continuous-wave self-deflection effect in sodium vapor

G. A. Swartzlander, Jr., H. Yin, and A. E. Kaplan

Department of Electrical and Computer Engineering, The Johns Hopkins University, Baltimore, Maryland 21218

Received December 20, 1988; accepted March 21, 1989

Observations of the self-deflection effect for an asymmetrical continuous-wave laser beam in sodium vapor are described, and comparisons based on theoretical calculations are made. A self-bending angle as large as eight diffraction widths was recorded, and strong attenuation of the on-axis radiation due to self-bending was measured. At ~200°C the self-deflection angle increased linearly with beam power, and we determined that $(n_2)_{max} \simeq -10^{-7}$ cm^2/W for intensities below 220 W/cm^2. While numerical calculations, based on an inhomogeneously broadened two-level system, predict strong saturation of the self-bending effect, we observed only moderate saturation.

1. INTRODUCTION

When a light beam with an asymmetrical spatial-intensity profile propagates through a nonlinear refractive material, it can undergo self-bending (or self-deflection), as first described in Ref. 1 and experimentally verified in Ref. 2. This potentially useful self-action effect occurs because a nonlinear prism is induced in the beam path as a result of the asymmetrical profile. Various application schemes have been proposed, such as resonatorless optical bistability,[3] radiation protection, and power limiting[4,5]; applications such as optical switching and interconnecting are also feasible. What is more, by measuring the self-deflection angle as a function of intensity, one may readily determine the intensity-dependent refractive index $\Delta n(I)$ and thereby obtain nonlinear spectroscopic information, e.g., at near-resonance frequencies.[6–8]

Since the first observation of self-bending[2] in a NaCl crystal, experiments have been limited to the use of pulsed lasers and have resulted in time-integrated observations as well as other complications that prohibited a comprehensive study of the effect. Recently self-deflection angles smaller than the diffraction angle were observed by using long infrared pulses from a powerful CO_2 laser at 10.6 μm,[9] and some indication of steady-state self-bending has been reported in liquid crystals.[10] It is known, on the other hand, that alkali vapors, e.g., sodium vapor, have a large nonlinearity that allows one to observe self-action effects (such as self-focusing[11] and resonatorless optical bistability based on self-focusing[12]) in the cw regime. The experiments in Refs. 11 and 12 exploited the large nonlinearity in the vicinity of the D resonances of sodium vapor.

Most recently, we reported[13] a first observation of the *cw self-bending effect* with a distinctly resolved self-deflected peak of radiation (up to eight times the diffraction width) in sodium vapor in the vicinity of the D_2 resonance at $\lambda_0 = 589.0$ nm. In this paper we present more detailed data and calculations related to the results[13] and report our new results. In particular, the constant motion of the centroid of the intensity distribution of the beam (related to the conservation of the total transverse momentum) as well as an anomalously low saturation of the nonlinear refractive index were observed and compared with models. In our experiment large self-bending angles were observed, and strong attenuation of the on-axis radiation was detected. In addition, the centroid of the intensity distribution in the far-field area was shifted by a significantly smaller angle than the self-deflection angle; we attribute this to the general principle of the conservation of transverse momentum. These results suggest a strong potential for applications, such as radiation protection and similar devices that perform rapid angular beam scanning. A short sodium-vapor cell was used so that the beam would not suffer significant diffraction within the interaction region. We found that when the laser was tuned just below the D_2 resonance frequency, the nonlinear refractive index was predominantly Kerr-like, i.e., $\Delta n = n_2 I$, with $n_2 \sim -10^{-7}$ cm^2/W. This result was not quite expected because a calculation of the saturation of the anomalous dispersion, based on the power-broadened hole-burning model,[7,8] predicts that $\Delta n(I)$ should be appreciably saturated under our experimental conditions.

This paper is organized in the following way. Sections 2 and 3 address some basic considerations related to self-bending and the motion of the centroid of the intensity distribution, respectively, whereas Sections 4 and 5 describe the experimental layout and results, respectively. In Section 6 we compare our results with a two-level model.

2. FAR-FIELD SELF-BENDING DUE TO A THIN NONLINEAR LAYER

An ideal case of self-bending occurs when a slab beam, with a spatial intensity profile that is right triangular [$I(x) = I_0(1 - x/w_0)$, $0 < x < w_0$, where x is the coordinate across the slab beam and w_0 is the beam size], propagates through a thin Kerr-like nonlinear medium,[1,4,5] as shown in Fig. 1. A nonlinear prism is induced in the beam path when the slope of the intensity profile, I_0/w_0, is sufficiently large. The beam will be self-deflected in the far-field region by the angle θ_{NL}, which can be expressed as[1,5]

$$\theta_{NL}/\theta_D = -n_2 k L I_0/2, \tag{1}$$

where k is the wave number, $\theta_D = 2/kw_0$ is a measure of the (half-) diffraction angle, and L is the thickness of the medium. Most applications of the self-bending effect will require a sufficiently resolved deflection: $|\theta_{NL}/\theta_D| > 1$. Similarly, the self-deflection angle of the half-Gaussian slab

0740-3224/89/071317-09$02.00

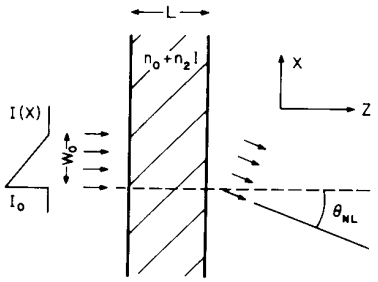

Fig. 1. Right-triangular intensity profile, of size w_0 and peak intensity I_0, is incident upon a thin nonlinear-refractive medium ($n = n_0 + n_2 I$) of length L. A nonlinear prism is induced in the medium, causing the transmitted rays to be deflected by an angle θ_{NL}.

beam, whose intensity profile is given by $I(x) = I_0 \exp(-2x^2/w_0^2)$, $x > 0$, is nearly equivalent to Eq. (1).[5] From an experimental viewpoint, however, one must consider three-dimensional rather than slab (or two-dimensional) beams.

In our experiment a three-dimensional TEM_{00} Gaussian beam of power P_{in}, as shown in the inset of Fig. 2, was used to achieve a large peak intensity, $I_0 = 2P_{in}/\pi w_0^2$. Half of the beam was covered with a razor blade to form a cross-sectional beam profile that was half-Gaussian along the x axis and symmetrical along the y axis. As the beam propagated along the z axis through the nonlinear medium, it was self-deflected away from the razor edge, i.e., the yz plane.

For this half-TEM_{00}, or semi-Gaussian, beam profile, it can be shown that Eq. (1) still gives a good approximation of the far-field self-bending angle. This can be understood by first considering a semiconic intensity profile, i.e., the three-dimensional analog of a triangular slab beam. This intensity profile is represented in circular coordinates by $I(r, \phi) = I_0(1 - r/w)$, for $-\pi/2 < \phi < \pi/2$ and $0 < r < w$, where r and ϕ are related to the Cartesian coordinates by $x = r\cos\phi$ and $y = r\sin\phi$. The nonlinear medium redirects the wave fronts of the beam, and in this case each portion of the beam contained within an angular increment, $d\phi$, will be radially self-deflected. Thus, for large z, the part of the beam lying in the xz plane originates from the initial beam in the neighborhood near $\phi = 0$. Using the Fourier-transform relationship between the transmitted and far-field electric fields, the intensity profile of the beam can be calculated and the self-deflection angle determined. The intensity profile along the x axis (with $y = 0$) in the far-field area is given by

$$I(\theta_x, 0) \propto \left| \int_0^w r dr (1 - r/w)^{1/2} \exp(-i n_2 I_0 k L r/w) \times \int_{-\pi/2}^{\pi/2} d\phi \exp(-ik\theta_x r\cos\phi) \right|^2,$$

where, making use of the paraxial approximation, we express $\theta_x \simeq x/z$. Noting that the second integrand oscillates rapidly when $(kr\theta_x) \gg 1$, except near $\phi = 0$, we make the approximation $\phi \simeq 0$ to evaluate the integral when the self-deflection angle is large, as we had anticipated. Hence, in the vicinity of large values of $(k\ r\ \theta_x)$, the exponential terms (which reveal the self-deflection angle) are identical to those obtained for a slab-beam profile.[5] In short, the angle of self-deflection is still approximately given by Eq. (1) when the intensity profile is half-conic and the deflection angle is large. At this point we can extrapolate to the case of a half-TEM_{00} beam. Analogous to the slab-beam case in which a Gaussian profile resembles a triangular intensity profile, now a TEM_{00} beam can be considered almost conic. As a result, the self-deflection angle of a half-TEM_{00} beam will also be approximated (and somewhat overestimated) by Eq. (1).

The application of Eq. (1) requires that the nonlinear refractive index of the medium be Kerr-like: $\Delta n(I) = n_2 I$. There are several ways to verify this experimentally. According to Eq. (1), if a linear relationship is found between θ_{NL} and P_{in}, then $\Delta n = n_2 I$ will be verified. On the other hand, if Δn is saturating as the power increases, then θ_{NL} will also saturate.

Another method of inspecting $\Delta n(I)$ is to record the far-field intensity at a point on the optical axis as the input power is increased. A graph of these two parameters will have a signature that depends on the functional form of $\Delta n(I)$. If the medium is thin and Kerr-like, and if the beam has a half-TEM_{00} profile, then an analytic solution can be found for the far-field on-axis intensity, $I_{on\text{-}axis}$. Again we make use of the Fourier-transform relationship between the near and far electric fields. However, since we are concerned only with the on-axis portion of the far-field beam, only the dc component of the Fourier integral needs to be evaluated. Thus the far on-axis electric field is expressed, up to a factor proportional to $1/z$, by

$$\xi_{on\text{-}axis} \propto \int_{-\pi/2}^{+\pi/2} d\theta \int_0^\infty r dr I_0^{1/2} \exp(-r^2/w_0^2) \times \exp[-i n_2 k L I_0 \exp(-2r^2/w_0^2)]. \quad (2a)$$

This integral coincides exactly with the integral used earlier in the theory of self-focusing of a completely symmetrical TEM_{00} beam[14]; using this solution, the far-field on-axis intensity is given by

$$I_{on\text{-}axis} \propto [C^2(\eta_{NL}) + S^2(\eta_{NL})] w_0^4/n_2 k L, \quad \eta_{NL} = (2n_2 k L I_0/\pi)^{1/2}, \quad (2b)$$

where C and S are the Fresnel integral functions.[15] Both of these methods, i.e., measuring the self-bending angle versus input intensity on the one hand and measuring the on-axis intensity versus input intensity on the other hand, can be

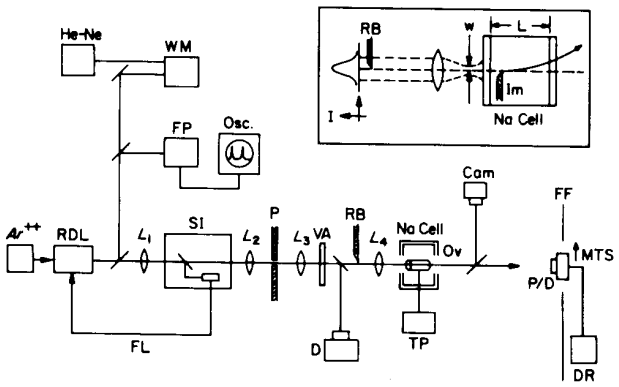

Fig. 2. Schematic diagram of the experiment. See the text for a complete description. The inset shows a razor blade inserted into the beam to form a semi-Gaussian beam profile, which is then imaged into the sodium cell of length L. The beam is self-deflected away from the razor image because $n_2 < 0$.

employed to extract n_2 from the experimental data and determine whether higher-order nonlinear terms are contributing to $\Delta n(I)$.

It should be emphasized, however, that Eq. (1) is valid only when the thickness of the nonlinear medium is small in comparison with the characteristic diffraction and self-(de) focusing lengths. Our experiment partially satisfied the thinness requirement because the length of the nonlinear medium (L = 18 mm) was much less than the diffraction length, $R_D = kw_0^2/2$ ($\simeq$260 mm). One of the advantages of self-bending is that it can be observed by using a negative nonlinear coefficient, n_2, which allows one to avoid complications related to self-focusing, in particular, the near-collapse of the beam. Our experiment was typically done on the self-defocusing side of the resonance in sodium vapor. For the largest product $|n_2|I$ in our experiment, the self-defocusing length, $R_{\mathrm{NL}} = w_0/2(|n_2|I_0)^{1/2}$, was of the same order as the cell length, L, which should have resulted in somewhat underestimated values of n_2 at large intensities. Indeed, the self-bending angle θ_{NL} appeared to saturate at large values of $|n_2|I$. Meanwhile the condition of uniform absorption across the beam was expected to be satisfied because the absorption saturates at an intensity 3 to 4 orders of magnitude smaller than those in this experiment.[6,7,11] The saturation intensity for a two-level system is given by $I_s = 2\pi hc/\lambda_0^3\tau_{\mathrm{N}}$ = 37.5 mW/cm^2, where τ_{N} is the natural lifetime of the transition.

3. CONSIDERATIONS OF THE CENTROID OF THE INTENSITY DISTRIBUTION

One of the important aspects of the self-deflection experiment is to make sure that it is really based on the nonlinear refractive index rather than on other nonlinear phenomena, such as nonlinear absorption and parametric processes. In order to verify this, and to provide another, although indirect, confirmation of our theory of self-deflection, we introduce here a method based on the conservation of the transverse momentum of the field. It is well known that the equation describing the propagation of two-dimensional light beams in Kerr-nonlinear materials, i.e., the cubic Schrödinger equation[16]

$$2ik\partial E/\partial z = \partial^2 E/\partial x^2 + k^2(\epsilon_2/\epsilon_0)|E|^2E, \tag{3}$$

has an infinite number of invariants (or constants of motion),[17] i.e., quantities obtained by integration of a field variable (field amplitude and its higher derivatives) over the transverse coordinate x; these quantities remain invariant along the propagation axis z. The first two invariants have clear physical meanings. One of them is the total power carried by the beam

$$\int_{-\infty}^{+\infty} |E(x, z)|^2 \mathrm{d}x = C_1 = \mathrm{inv}. \tag{4}$$

The other one may be regarded as the total transverse momentum of the field and can be written in the form

$$(2ik)^{-1} \int_{-\infty}^{+\infty} (EE_x^* - E^*E_x)\mathrm{d}x = C_2 = \mathrm{inv}, \tag{5}$$

where $E_x = \partial E/\partial x$. It has also been shown[18] that at least three invariants, including the two above, also exist for a transparent nonlinear material with an *arbitrary* nonlinearity [i.e., with $f(|E|^2)$ instead of $|E|^2$ in Eq. (3), where f is an arbitrary function of $|E|^2$]; it has also been shown that the two invariants above have precisely the same form as that for a Kerr nonlinearity. These two conservation laws are also valid for linear media, and they have a universal character for the propagation of the beam in all nonabsorbing materials. It is obvious that these invariants of motion are generally invalid for systems with absorption (linear and nonlinear). The law of conservation of transverse momentum, Eq. (5), essentially implies that the (diffracting) beam as a whole propagates strictly along a straight line, even in a medium with a nonlinear refractive index, i.e., that the intensity distribution

$$x_c \equiv \int_{-\infty}^{+\infty} x|E(x)|^2\mathrm{d}x/C_1 \tag{6}$$

propagates rectilinearly, which means that $\mathrm{d}x_c/\mathrm{d}z$ = constant. Indeed, by using the definition, Eq. (6), we obtain

$$C_1\mathrm{d}x_c/\mathrm{d}z = \int_{-\infty}^{+\infty} x\mathrm{d}x(E^*E_z + EE_z^*)$$

$$= \int_{-\infty}^{+\infty} \mathrm{d}x(x/2ik)(E^*E_{xx} - EE_{xx}^*),$$

where we used Eq. (3) to evaluate E_z through E_{xx} [note that this transformation is valid for arbitrary nonlinearity, not only to Kerr nonlinearity, $\Delta n \propto |E|^2$ as in Eq. (3)]. Integrating the latter expression by parts, we obtain

$$\mathrm{d}x_c/\mathrm{d}z \propto x(E^*E_x - EE_x^*)\Big|_{-\infty}^{+\infty} - \int_{-\infty}^{\infty} (E^*E_x - EE_x^*)\mathrm{d}x.$$

On the right-hand side of this relation, the term $x(E^*E_x$ − c.c.)$|_{-\infty}^{+\infty}$ is equal to zero since any quadratic form of the far-axis field vanishes faster than $1/x$ as $|x| \to \infty$ [i.e., in this case $|E^*E_x| = o(1/x)$], which is basically due to the fact that total power of the beam (i.e., $\int_{-\infty}^{\infty} |E|^2\mathrm{d}x$) is finite. Thus

$$\mathrm{d}x_c/\mathrm{d}z \propto \int_{-\infty}^{\infty} (E^*E_x - EE_x^*)\mathrm{d}x = \mathrm{const.}, \tag{7}$$

and we find that

$$x_c = zc_2/c_1 + x_c(z = 0), \tag{8}$$

by virtue of the conservation of the total transverse momentum of the field, Eq. (5). Since the total transverse momentum conservation is valid not only for Kerr-like nonlinearity but also for *arbitrary* nonlinearity[18] [i.e., with $\Delta n = f(|E|^2)$, where $f(\xi)$ is an arbitrary function of ξ], the rectilinear propagation of the centroid of the intensity distribution, Eq. (8), remains valid for arbitrary nonlinearity as well. In the simplest case, when a beam is normally incident upon a nonlinear layer, the transverse momentum is equal to zero, and the centroid of the intensity distribution remains fixed along the incident line of propagation.

This transverse momentum conservation seems to suggest the absence of the self-bending effect. A simple consideration shows, however, that this is not true as far as the propagation of the strong *peak* in the nonlinearly diffracted beam is concerned. If, because of an asymmetrical intensity profile, a strong peak in the beam is formed that moves away from the propagation axis, say to the right, as the beam propagates through the nonlinear material, then a long, but low-intensity, tail will extend on the left-hand side of the

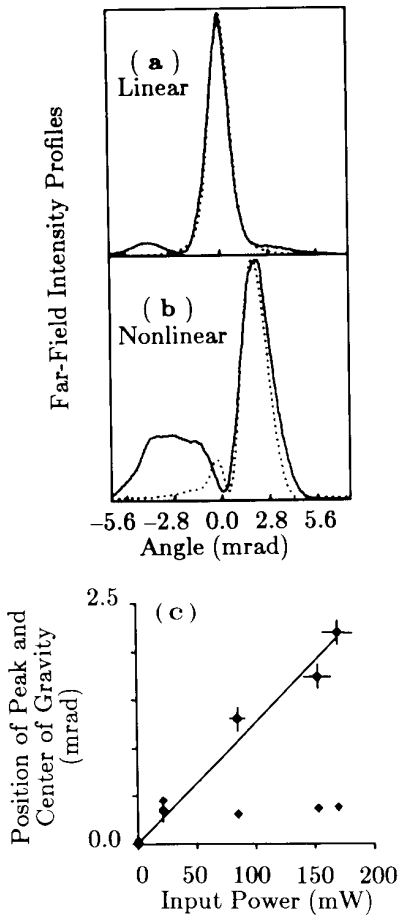

Fig. 3. Far-field intensity profiles obtained at 202°C are shown by the solid curves for both linear (a) and nonlinear (b) propagation. Numerical calculations based on a slab-beam/thin-film analysis are shown as dotted curves. (c) The self-deflection angle is plotted against the input beam power (circles with error bars). The linear relationship indicates that $\Delta n = n_2 I$, where $n_2 = -1.4 \times 10^{-7}$ cm^2/W. The centroid of the intensity distribution of each of the measured profiles is marked with a diamond.

propagation axis that provides a counterbalance for the strong peak on the right; thus the centroid of the intensity distribution (or transverse momentum) of the beam remains fixed.

Although the energy and transverse momentum invariants above were found, strictly speaking, for a slab (or two-dimensional) beam, it is clear that at least these two invariants will be valid for the three-dimensional case, or at least in the situation when the main perturbation in the beams occurs only along one of the transverse coordinates, as for the case of self-deflection. Therefore this phenomenon suggests an interesting experimental method of verifying whether the nonlinear interaction due to the nonlinear refractive index takes place. This procedure has been used by us in our experiments; in each case when the intensity profile in the far field has been measured, in addition to the spatial shift of the main intensity peak we have determined the position of the centroid of the intensity distribution, which has been accomplished by simply integrating across the recorded profiles.

The results indicating the position of the centroid of the intensity distribution of the beams are shown on all the experimental plots; see Figs. 3(c), 4(c), and 5. One can see that the centroids are amazingly stationary, i.e., the measured shift of the centroid of the intensity distribution has always been much smaller than the shift of the self-deflected peak. Indeed, for example in Fig. 3(b) the deflection of the main strong peak to the right-hand side is accompanied by the formation of a very broad plateau with a much smaller peak intensity. The shift of the centroid of the intensity distribution is substantially smaller than the shift of the deflected peak. This result was observed in both situations, when we changed the intensity of the beam for a fixed detuning frequency and when we changed the detuning frequency for a fixed intensity. This shows that the nonlinear absorption had affected the observed effect to a small degree, if at all. This suggests that the saturation of absorption was high, even in the peripheral areas of the beam (if the absorption were different across the beam, the total transverse momentum of the beam, as well as the position of the centroid of the intensity distribution, would not be conserved). The calculated profiles shown by the dotted curves in Figs. 3

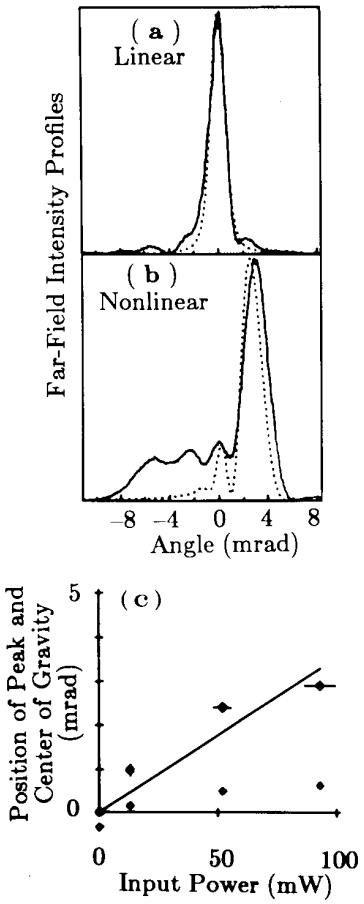

Fig. 4. Experimental results obtained at 212°C are shown by the solid curves for both linear (a) and nonlinear (b) propagation. Results of our numerical calculations are depicted by the dotted curves. (c) Self-deflection angle plotted against the input-beam power (circles with error bars). Rather than increasing linearly with intensity (solid curve), the self-deflection effect apparently saturates. The centroid of the intensity distribution of each of the measured profiles is marked with a diamond.

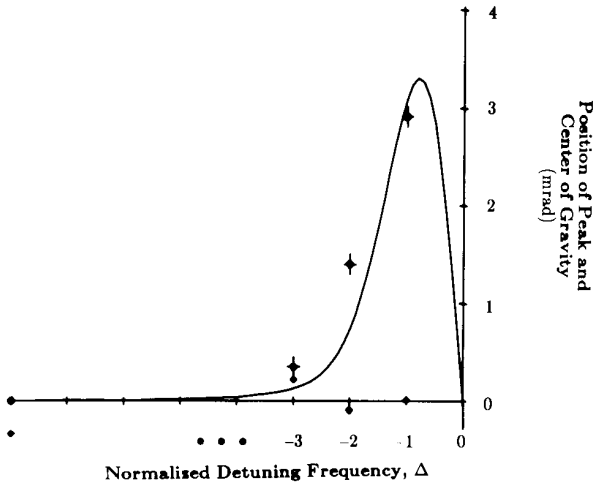

Fig. 5. Self-deflection angle as a function of the normalized detuning frequency. The experimental data are represented as circles with error bars. The solid curve is a numerical calculation that is discussed in the text. The diamonds indicate the position of the centroid of the intensity distribution of the profiles.

and 4 also follow this conservation law. In the nonlinear cases the strong self-deflected peak is counterbalanced by the distribution on the opposite side of the axis, which forms a long (although low-intensity) tail that extends beyond the border of the figure.

4. EXPERIMENTAL LAYOUT AND TECHNIQUES

Figure 2 is a schematic of the experimental setup. A Coherent argon-ion laser (514.5 nm, ~7 W) was used to pump the dye Rhodamine 6G in a Spectra-Physics ring dye laser (RDL). In this device, frequency-stabilized, single-mode operation was accomplished through a feedback loop (FL) to the laser cavity from a pair of stabilizing interferometers (SI). The beam was linearly polarized in the horizontal plane (normal to the figure).

The gross dye-laser wavelength was measured with a homemade interferometric wavemeter (WM) and a single-frequency helium–neon laser (He-Ne). The laser frequency was tuned until the maximum resonant radiation, hereafter called the reference frequency, ν_{ref}, was observed. This frequency could be identified to within better than ±0.1 GHz with the aid of a 2-GHz scanning Fabry–Perot interferometer (FP) and an oscilloscope (Osc.) and was believed to be insensitive to changes in temperature. The laser frequency was then detuned below the resonance frequency until the strongest self-bending effect was seen—typically 1.9 GHz from the reference frequency, as measured with the Fabry–Perot interferometer.

The laser beam was directed through a series of lenses: a collimating lens (of focal length L_1 = 30 cm), another lens (L_2 = 30 cm) that focused the beam upon a 100-μm spatial filter pinhole (P), and another collimating lens (L_3 = 30 cm) that passed the beam through a variable attenuator (VA). The pinhole was used as a weak spatial filter and reduced the beam power by 6%.

A razor blade (RB) was mounted on a translation stage and could be inserted into the beam at its minimum spot size (waist) to obscure half of the beam, thereby forming a semi-Gaussian beam profile. The semi-Gaussian profile was imaged into the sodium (Na) cell with an imaging lens (L_4 = 10 cm). The transformed waist formed by L_4 occurs slightly closer to L_4 than the image plane of the razor. Since the beam size w_0 [see the text following Eq. (1)] was quite large (220 μm ± 15%), the exact location of the waist was not well determined, although it did occur near, but before, the entrance of the cell. In general the location of the waist and the razor image plane are not coincident, and care must be taken to account for their relative positions; the direction of self-bending can be reversed if the image plane precedes the plane of the waist. The inset of Fig. 2 shows the Gaussian input beam in the plane just before the beam is cut. The values of power given throughout this paper will refer to the unobscured beam power in this plane, measured by the detector, D.

L_4 also serves several other purposes. First, the beam size in the sodium vapor must be small enough to create a large peak intensity; otherwise nonlinear effects will not be observable. Also, the beam size should be large enough that, as the beam propagates through the sodium cell, diffraction does not severely distort the semi-Gaussian profile. The diffraction problem can be critical because the high-spatial-frequency components of the razor image can become quite intense, leading to undesirable nonlinear self-action effects, which accelerate the destruction of the semi-Gaussian profile as it propagates. This is especially troublesome if the laser is tuned to the self-focusing side of the resonance where $n_2 > 0$. (The propagation of a slab beam through a finite self-focusing nonlinear medium can be solved numerically by applying the so-called split-step Fourier method[19] to the nonlinear Schrödinger equation; we found that some adverse diffraction effects could be reduced if the beam is diverging at the image plane, as will be reported elsewhere.)

The sodium vapor was contained in an 18-mm-long, 25-mm i.d. borosilicate (Corning 7056) cell, which was sealed under vacuum. The windows were wedged to prevent back-reflections and were nominally 6.3 mm thick. The cell walls extended past the windows to help maintain their temperature uniformity. The sodium was heated in an oven (Ov), and temperature probes (TP) were used to monitor the temperature of both the main body and the finger of the cell. The main body of the cell was wrapped with heating tape, which was powered by a variable ac generator. The side reservoir or finger on the cell contained purified sodium and was wrapped with nickel heating wire, which was energized by another variable ac generator. The temperature of the main body of the cell was maintained ~20°C higher than the finger to prevent condensation on the windows. The finger temperature, which determines the vapor density, was accurate to within ~2°C.

After passing through the sodium vapor, the beam propagated to the far-field region (~95 cm, or roughly four diffraction lengths), where intensity profiles were made by using a pinhole/detector arrangement (P/D) mounted on an Oriel motorized translation stage (MTS). This enabled us to average over repeated measurements taken with a digital recorder (DR). The silicon photodiode was covered with a small pinhole (5–50 μm) so that a narrow strip of the far-field profile could be measured. The 1-Hz low-pass filter was used to eliminate laser power fluctuations (±10%) from the

photodiode signal. The far-field beam profiles (FF) were also recorded with a polaroid camera (Cam).

Special care was taken when we measured the profiles for the linear case. Since a low-power beam at a near-resonant frequency encounters strong absorption, the linear profiles had to be made with the laser tuned far off-resonance. Under linear propagation the beam was not found to be deflected as the laser frequency was tuned. Similar tests showed that the variable attenuator (Newport), which was used to vary the beam power, introduced a small shift of the beam position as the attenuator was translated. This shift increased with increasing translation distance, up to ~0.5 mrad across the entire length of the attenuator. A smaller portion of the attenuator was used in our experiment, and the actual shifts encountered were relatively small.

The self-bending angle was determined in the following way. First the far-field angular beam width was measured for a Gaussian and a semi-Gaussian beam. In the former case we obtained the diffraction angle, θ_d. As expected, a comparison of these two profiles showed that the (half-) diffraction angle, θ_d, was measured to be approximately four times smaller than the full angular width of the diffracted semi-Gaussian beam (measured at e^{-2} times the peak intensity). This enabled us to omit the direct measurement of θ_D, since removing the razor is not always desirable if one wants to retain the same configuration of the beam-and-razor system. The profiles of the self-deflected beams at various beam powers were then made, and self-deflection angles were calculated.

5. EXPERIMENTAL RESULTS

A number of self-deflected beam profiles were measured under various conditions, e.g., at different input powers, vapor densities, and laser frequencies. Self-bending became visually obvious near 197°C (or at an atomic density of $N = 2.6 \times 10^{12}$ cm^{-3}), with an input beam power of 170 mW. The linear (off-resonance) and nonlinear (near-resonance) beam profiles under these conditions are shown in Fig. 6(a). To highlight its shape, the self-deflected beam (dashed curve) has also been rescaled as shown in Fig. 6(b). The self-deflection angle was 1.6 mrad or $\theta_{NL}/\theta_D \simeq 2.3$. The existence of the subpeak occurring on the opposite side of the central position is expected from the Kerr-nonlinear model, but it is much broader than one would expect from a simple slab-beam analysis. It may be due to the three-dimensional nature of the beam, diffraction within the sodium cell, and the diffusion of excited atoms, particularly at the edge of the beam. Assuming that Δn is Kerr-like, we obtain from Eq. (1) that $n_2 = 1.1 \times 10^{-7}$ cm^2/W (±30%). When the magnitudes of the two beams in Fig. 6(a) are compared, it is clear that the near-resonance beam suffered considerable absorption, although we did not investigate whether the absorption is saturated, as expected.

By increasing the temperature, and thus the vapor density, a larger nonlinearity was achieved. In the data shown in Fig. 3 the temperature was increased to 202°C ($N = 3.6 \times 10^{12}$ cm^{-3}). At an input power of 170 mW, the self-deflected peak, shown in Fig. 3(b), was displaced by 2.1 mrad ($\simeq 3.0\ \theta_D$) with respect to the linear beam in Fig. 3(a). To test whether Δn is Kerr-like at this temperature, we have measured the self-deflection angle at a variety of input beam powers. Figure 3(c) shows that the relation between the deflection angle and the input power is linear: $\theta_{NL} = (12.6$ mrad/W ± 5%)P_{in}, indicating that Δn is Kerr-like, with $\langle n_2 \rangle = (\theta_{NL}/\theta_D P_{in})(\pi w_0^2/kL) = -1.4 \times 10^{-7}$ cm^2/W (±20–30%). In comparison with the value measured in Fig. 6, n_2 has increased roughly in proportion to the vapor density N, as expected (see Section 6). The centroids of the intensity distribution of the profiles were identical to each other within ±0.2 mrad.

As stated above, the position of the peak can be approximated based on the analysis of a slab half-Gaussian beam. The dotted curves in Figs. 3(a) and 3(b) show the computed profiles. Using the value of n_2 obtained above, we see that the computed self-deflection peak agrees with the actual peak. The slab-beam analysis is not valid in the vicinity of $\theta \approx 0$. It should, however, apply to the counter-self-deflected components occurring at large values of θ. The agreement is poor because diffraction and nonlocal effects were not considered in the slab model.

A similar set of measurements was also made at 212°C ($N = 6.3 \times 10^{12}$ cm^{-3}). Figures 4(a) and 4(b) show the linear (off-resonance) and self-deflected far-field profiles, respectively. The dotted curves again show the profiles computed for a slab beam. Figure 4(c) shows the measured relationship between the self-deflection angle and the input-beam power. The linear fit gives $\theta_{NL} = (35$ mrad/W ± 11%)P_{in}, from which we obtain $\langle n_2 \rangle = 4 \times 10^{-7}$ cm^2/W (±20–30%). The correlation is not so good as that for Fig. 3(c), which is apparently attributed to the fact that the characteristic self-defocusing length R_{NL} is comparable with the cell length L, causing θ_{NL} to saturate, as seems obvious from Fig. 4(c), which shows the tendency of the measured angles to level off with increasing input power. There may also be a contribution from the saturation of Δn. In contrast to the low-

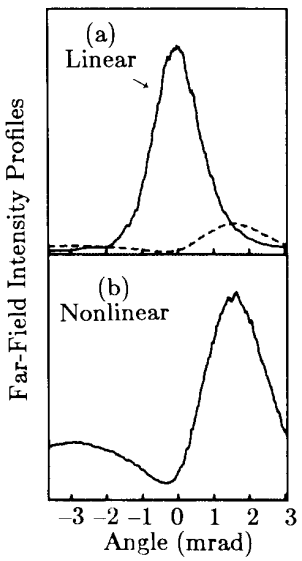

Fig. 6. Far-field intensity profiles across a narrow slice of the beam cross section are plotted. The liquid-sodium temperature was 197°C. The peak of the self-deflected beam, shown as the solid curve in (b), is offset from the peak of the linearly propagated beam, shown as the solid curve in (a), by 1.6 mrad. The dashed curve shows the magnitude of the self-deflected profile, measured at a near-resonant frequency, in comparison with the linear profile measured at an off-resonant frequency.

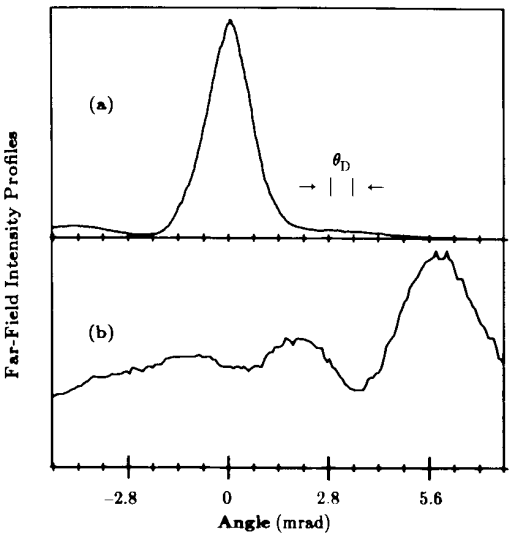

Fig. 7. A large self-deflection angle, measuring $8.4\theta_D$, was achieved at 214°C. The linear (a) and nonlinear (b) profiles have been arbitrarily normalized.

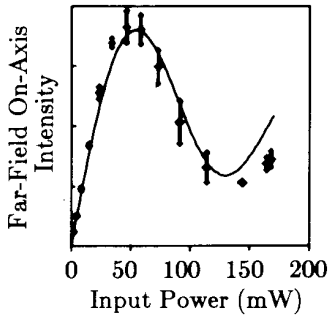

Fig. 8. The on-axis far-field beam intensity is plotted against the input beam power. The solid curve is a fit to the analytical solution for a Kerr-nonlinear medium, with $n_2 = -1.7 \times 10^{-7}$ cm^2/W.

temperature data, n_2 apparently increases faster than the vapor density, N, at this elevated temperature. The centroids of the intensity distribution of the profiles were identical to each other within ±0.4 mrad.

Larger self-deflection angles were also observed at higher temperatures. For example, at 214°C ($N = 7.0 \times 10^{12}$ cm^{-3}) and with an input-beam power of 170 mW, a self-deflection angle of 5.9 mrad or 8.4 θ_D was measured, as shown in Fig. 7. The nature of the nonlinearity at such high temperatures was not investigated because (1) the absorption was quite strong, making measurements difficult, and (2) the rate of sodium attack on the cell was large at this temperature.

Another way of observing the effect and comparing it with the theory is to measure the far-field on-axis radiation. In this experiment we observed the intensity of radiation at the point that corresponds to the center of the *linear* beam. According to Eq. (2), after achieving a maximum value, the intensity is expected to decrease as self-deflection occurs and then oscillate as secondary peaks and troughs are formed as the input power increases. The results of this experiment are shown in Fig. 8. The solid curve is a fit of the data of Eq. (2), in which the amplitude and n_2 ($=-1.7 \times 10^{-7}$ cm^2/W) are the fitting parameters. The temperature was 195°C ($N = 2.5 \times 10^{12}$ cm^{-3}), beam powers of up to 170 mW were used, and the detuning was 2.0 GHz. In extrapolating the previous experimental value of $n_2 \simeq -1.4 \times 10^{-7}$ cm^2/W to the lower vapor density, a value of $n_2 \simeq -1.0 \times 10^{-7}$ cm^2/W was expected. The factor-of-1.7 discrepancy can be attributed to several sources of error, including the underestimation of n_2 when Eq. (1) is applied to a semi-Gaussian beam and the omission of absorption and self-defocusing.

6. COMPARISON OF EXPERIMENTAL RESULTS WITH A TWO-LEVEL MODEL

Thus far we have not discussed the dispersive property of the nonlinear refractive index, which may be used with the self-bending effect to achieve fast angular scanning by varying the laser frequency rather than the power. In this section we will examine this phenomenon and discuss nonlinear dispersion in terms of a two-level model.

Self-deflection profiles obtained at different laser frequencies are shown in Fig. 9, where a self-deflection angle of 2.6 mrad was achieved over a 2-GHz laser frequency range. Here the liquid-sodium temperature was 212°C, and the beam power was constant (~120 mW). The onset of saturation of the self-bending angle θ_{NL} is evident at this power [see the discussion of Fig. 4(c) in Section 5]. In the linear case (A), the profile was obtained at a far-off-resonance frequency, and the diffraction width was determined to be 0.74 mrad. The other profiles (B, C, and D) were measured at −3.9, −2.9, and −1.9 GHz, respectively, from the middle of the resonance. At smaller detuning frequencies the self-bending angle decreased, and the absorption was quite strong. The inset of Fig. 9 shows the relative magnitudes of each of the near-resonant profiles. In spite of the larger absorption closer to the resonance, the strongest self-deflected beam (D) is clearly distinguished from the tail of the nearly undeflected beam (B).

To gain an understanding of nonlinear dispersion, we have made numerical calculations of the refractive index, based on a model in which sodium vapor is treated as an inhomogeneously broadened two-level system.[7,8] According to this model the refractive index $n(\nu, I)$ varies with the excitation frequency ν and the intensity I as

$$n(\nu, I) - 1 = -\delta n \, \mathrm{Im}[w(\Delta + i\eta)], \tag{9}$$

where $\delta n = (\ln 2)^{1/2}\lambda^3 N/(16\pi^{5/2}\tau_N \Delta\nu_D)$ and the absorption of

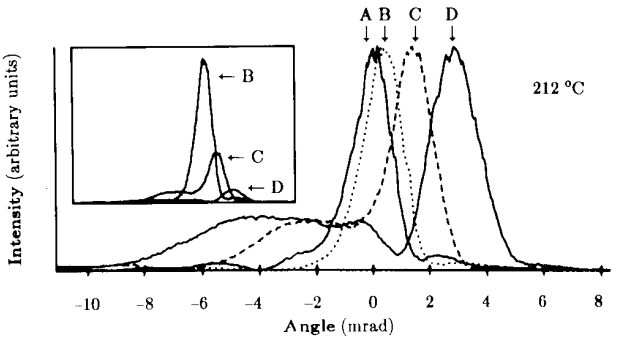

Fig. 9. The normalized profiles of self-deflected beams that were obtained at different laser frequencies are shown, and their relative magnitudes are depicted in the inset. The beam centered at zero (A) was measured far off-resonance, and the others (B, C, and D) were measured at −3.9, −2.9, and −1.9 GHz, respectively, from the resonance.

the field E along the axis of propagation, z, is determined by the equation

$$E^{-1}\mathrm{d}E/\mathrm{d}z = -2\pi\nu\delta n(1 + I/I_s)^{-1/2}/c \times \mathrm{Re}[w(\Delta + i\eta)], \quad (10)$$

where $\Delta n = n(\nu, I) - n(\nu, 0)$ is the nonlinear change of the refractive index, $\Delta = 2\sqrt{\ln 2}(\nu - \nu_0)/\Delta\nu_D$ is the normalized detuning frequency, $\eta = a(1 + I/I_s)^{1/2}$ is the power-broadened hole size, and w is the error function for complex arguments. The inset of Fig. 10(a) shows the real (curve 1) and imaginary (curve 2) parts of the error function for complex arguments, $\mathrm{Re}[w]$ and $-\mathrm{Im}[w]$. The dashed lines (curves 1′ and 2′) show the values for these components under saturation. The dispersion curve ($-\mathrm{Im}[w]$) shows that the nonlinear refractive index is greatest at $|\Delta| \sim 1$. For sodium vapor, we compute $\delta n \simeq 2.7 \times 10^{-17} N$ (cm^{-3}), where N is the atomic density, $\tau_N = 16.3$ nsec is the natural lifetime,[20] $\Delta\nu_D = 2\nu_0[2kT(\ln 2)/m_a c^2]^{1/2} \simeq 1.66$ GHz is the Doppler linewidth (with k and m_a equal to Boltzmann's constant and the mass of the atom, respectively), and the ratio of the natural and Doppler widths is $a = \sqrt{\ln 2}/\pi\tau_N\Delta\nu_D \simeq 9.85 \times 10^{-3}$. According to the model, the absorption coefficient saturates at $I_s = 2\pi hc/\lambda_0^3\tau_N = 37.5$ mW/cm^2, which is several orders of magnitude smaller than the intensities used in the experiment. Because we operate at 10^3 times this value, nonlinear absorption is not expected to affect the intensity profile of the beam significantly. This was also confirmed by our qualitative observations.

As expected from this model, the self-deflection angle was observed to change its sign when the laser frequency was tuned to opposite sides of the resonance. In addition, the strongest nonlinear effect was observed in the vicinity of $|\Delta| = 1$, which was also expected. On the other hand, the observed saturation of θ_{NL} is much weaker than the calculated saturation of the refractive index, which is shown in Fig. 10(a). And, while the observed self-deflection profiles exhibited the generation of subpeaks, which are characteristic of a Kerr-like nonlinearity, i.e., little or no saturation of Δn, the profiles calculated using the saturated two-level model do not show subpeaks at all. This difference is demonstrated in Fig. 10(b), in which we have calculated the self-deflection profiles for saturated (solid curve) and Kerr-like (dotted curve) nonlinearities. Not only do the profiles differ but the relation between the self-deflection angle and the input-beam power differ for these two cases as well: θ_{NL} increases linearly with P_{in} for the Kerr case, while it increases somewhat logarithmically for the saturation case.

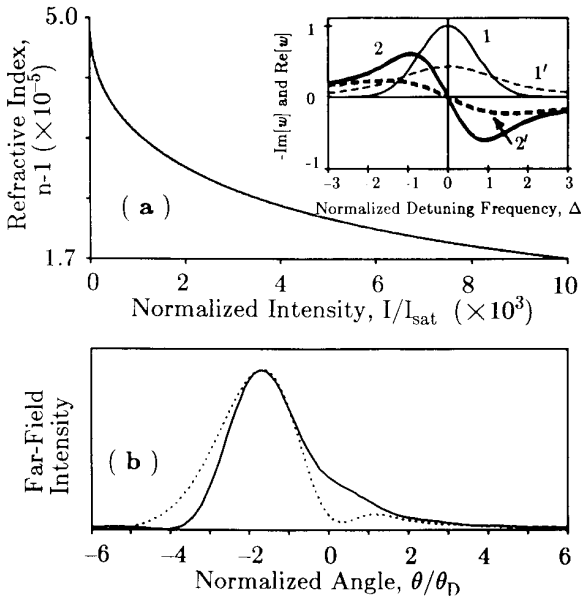

Fig. 10. (a) Treating sodium as an inhomogeneously broadened two-level system, we computed values of the intensity-dependent refractive index, $\Delta n(I)$, finding, in contrast to our experimental results, that strong saturation should occur. The inset shows the functions $\mathrm{Re}[w]$ (1) and $-\mathrm{Im}[w]$ (2) in their linear states, with their saturated states depicted by 1′ and 2′, respectively. As observed experimentally, our numerical calculations predict that the maximum nonlinear effect should occur at $\Delta \simeq -1$ (and $\Delta \simeq +1$). (b) A comparison of the self-deflected profiles of slab semi-Gaussian beams in saturated (solid curve) and Kerr (dotted curve) nonlinear media shows that a saturated nonlinear response does not produce subpeaks.

The discrepancies between the experimental data and the saturated two-level model are not too surprising, however, because the sodium D_2 resonance should be treated as a three-level system with optical pumping between the two hyperfine split (1.77-GHz) sublevels of the $^2S_{1/2}$ ground state.[11,21] When the laser frequency is on the self-defocusing side of the resonance, atoms in the higher-energy $F = 2$ state are more readily excited than those in the lower-energy $F = 1$ state. When the beam power is low, some atoms are optically pumped by spontaneous emission from the $F = 2$ level to the $F = 1$ level via the $^2P_{3/2}$ excited state. This can occur at a rate comparable to $1/\tau_N$. However, in the absence of collisions, the relaxation time of the optically pumped system can be quite long, thereby reducing the effective atomic density. As the beam power increases above the point where the rates of spontaneous and stimulated emission are equal, the transition becomes saturated, leaving the atoms favoring the decay into the $F = 2$ state by means of stimulated emission. As the power increases further, the hole burned in the line becomes power broadened, and there is a transition from an inhomogeneous line to a homogeneously broadened line.

The effects of optical pumping may be overcome by using circularly polarized light (we used only linearly polarized light). Other complications may also arise, such as nonlocal effects due to the drift of excited atoms[11] (contributing to the nonlinear refractive index) over an average distance of $\tau_N(3kT/m_a)^{1/2} \sim 10$ μm during the excited-state lifetime and long-range ($\sim$100 μm) light–light interactions[22] mediated by atoms moving under the action of a gradient force in the beam. These may significantly affect the profile of the refractive index at the edge of the half-TEM_{00} beam, causing the discontinuous edge to become rounded and leading to a larger-than-expected counter-self-deflected component. Also, the absorption coefficient at the edge will be affected owing to the diffusion of unsaturated atoms into this region. To some extent this is advantageous because the larger absorption will attenuate the high-spatial-frequency components of diffraction, which originate at this edge.

An expansion of w for large detuning ($|\Delta| \gg 1$) and small power broadening ($\eta \ll |\Delta|$) shows that the refractive index in Eq. (9) is Kerr-like under those conditions[8]:

$$\Delta n \approx n_2 I, \qquad n_2 = (\ln 2)^{3/2}\lambda^6 N/(32\pi^6\Delta^3 hc\Delta\nu_D{}^3\tau_N{}^2). \quad (11)$$

For example, at 202°C and a detuning of $\Delta = -1.0$, this

approximation gives $n_2 = -1.2 \times 10^{-7}$ cm^2/W. Surprisingly, this also agrees exceptionally well with the experimentally determined value [using Eq. (1)], in spite of violation of the inequalities ($|\Delta| \simeq \eta \simeq 1.0$). At higher temperatures, where θ_{NL} was observed to saturate, relation (11) was in poor agreement with the experimental data. The apparent temperature dependence of the saturation of θ_{NL} may arise because of internal self-action *within* the cell. Indeed, at higher temperatures, the characteristic self-defocusing length R_{NL} is comparable with the cell length L. Saturation of the refractive index may also be present, but, at least according to the two-level model, the saturation of the refractive index is relatively immune from temperature variations.

In Fig. 5 we have plotted the self-deflection angles of the profiles shown in Fig. 9 as a function of the normalized detuning frequency, Δ. Making use of Eq. (1), one may directly recover the nonlinear dispersion coefficient $n_2(\nu)$ from such a graph, assuming of course that the medium is thin and Kerr-like. When these conditions are not strictly satisfied, θ_{NL} will at least qualitatively track $\Delta n(\nu)$ as the frequency is varied. Because of the ground-state splitting, the resonant frequency ν_0 is not clearly defined. In the experiment we have referenced all detuning frequencies from the point that produced the brightest resonant radiation, ν_{ref}, which we assumed occurs midway between the $^2S_{1/2}$ ($F = 1$) to $^2P_{3/2}$ and $^2S_{1/2}(F = 2)$ to $^2P_{3/2}$ transitions. On the self-defocusing side of the resonance we are concerned primarily with the saturation of the latter transition. Thus we express the normalized detuning frequency as $\Delta \simeq [(\nu - \nu_{ref}) + 1.77\ \text{GHz}/2]2\sqrt{\ln 2}/\Delta\nu_D$, where 1.77 GHz corresponds to the separation of the hyperfine sublevels. For comparison with the two-level model, the nonlinear dispersion curve, Δn, is shown in Fig. 5 by the solid curve, which has been vertically scaled to obtain the least-squares error with respect to the experimental data. As stated above, the model correctly predicts that the nonlinear refractive index peaks near $\Delta = -1$.

7. CONCLUSION

In conclusion, we observed cw self-bending of a laser beam in sodium vapor, recording self-deflection angles up to eight times the diffraction angle of the input beam. This effect is strong enough to permit useful applications such as optical switching and limiting, optical bistability, and nonlinear coupling. We also observed the strong attenuation of the on-axis radiation resulting from the self-bending effect. Self-bending was observed at various beam powers, vapor densities, and detuning frequencies. The measured self-deflected profiles revealed a main self-deflected peak and smaller counter-self-deflected subpeak(s), characteristic of unsaturated Kerr-like nonlinear media, i.e., $\Delta n(I) = n_2 I$. From data obtained at 202°C, we determined that the maximum nonlinear coefficient is $n_2 \simeq -10^{-7}$ cm^2/W for near-resonant tuning on the self-defocusing side of the resonance. Although numerical calculations based on a two-level model showed that $\Delta n(I)$ was expected to exhibit strong saturation, the actually measured values of $\Delta n(I)$ did not show strongly pronounced saturation, which may be caused by optical pumping between the hyperfine split sublevels of the D_2 transition.

ACKNOWLEDGMENTS

We gratefully thank D. Elliott for his expert help with developing the laboratory, C. Harrington for lending his craftsmanship, and the Purdue University School of Electrical Engineering where this experiment was conducted. We are indebted to J. E. Bjorkholm for his insights on sodium-vapor experiments. We are grateful to both of the anonymous reviewers for their constructive and helpful comments. This research was supported by the U.S. Air Force Office of Scientific Research and the Indiana Corporation for Science and Technology.

REFERENCES AND NOTES

1. A. E. Kaplan, Pis'ma Zh. Eksp. Teor. Fiz. **9,** 58 (1969) [JETP Lett. **9,** 33 (1969)].
2. M. S. Brodin and A. M. Kamuz, Pis'ma Zh. Eksp. Teor. Fiz. **9,** 577 (1969) [JETP Lett. **9,** 351 (1969)].
3. A. E. Kaplan, Opt. Lett. **6,** 360 (1981).
4. J. A. Hermann, Opt. Commun. **62,** 367 (1987); Opt. Quantum Electron. **19,** 169 (1987).
5. G. A. Swartzlander, Jr., and A. E. Kaplan, J. Opt. Soc. Am. B **5,** 765 (1988).
6. A. Javan and P. L. Kelley, IEEE J. Quantum Electron. **QE-2,** 470 (1966).
7. D. H. Close, Phys. Rev. **153,** 360 (1967).
8. J. E. Bjorkholm, AT&T Bell Laboratories, Room 4B-423, Holmdel, New Jersey 07733 (personal correspondence).
9. I. Golub, Y. Beaudoin, and S. L. Chin, Opt. Lett. **13,** 488 (1988); J. Opt. Soc. Am. B **5,** 2490 (1988).
10. I. C. Khoo, R. R. Michael, T. H. Liu, G. Finn, and A. E. Kaplan, Proc. Soc. Photo-Opt. Instrum. Eng. **613,** 43 (1986); I. C. Khoo, G. M. Finn, R. R. Michael, and T. H. Liu, Opt. Lett. **11,** 227 (1986).
11. J. E. Bjorkholm and A. Ashkin, Phys. Rev. Lett. **32,** 129 (1974).
12. J. E. Bjorkholm, P. W. Smith, W. J. Tomlinson, and A. E. Kaplan, Opt. Lett. **6,** 345 (1981).
13. G. A. Swartzlander, H. Yin, and A. E. Kaplan, Opt. Lett. **13,** 1011 (1988).
14. J. H. Marburger, "Self-focusing: theory," in *Progress in Quantum Electronics,* J. H. Sanders and S. Stenholm, eds. (Pergamon, London, 1975), Vol. 4, p. 60.
15. See, for example, G. A. Korn and T. M. Korn, *Mathematical Handbook for Scientists and Engineers* (McGraw-Hill, New York, 1968), p. 820.
16. P. L. Kelley, Phys. Rev. Lett. **15,** 1005 (1965).
17. V. E. Zakharov and A. B. Shabat, Zh. Eksp. Teor. Fiz. **61,** 118 (1971) [Sov. Phys. JETP **34,** 62 (1972)].
18. R. H. Enns, S. S. Rangnekar, and A. E. Kaplan, Phys. Rev. A **35,** 466 (1987).
19. R. H. Hardin and R. D. Tappert, SIAM Rev. Chronicle **15,** 423 (1973); T. R. Taha and M. J. Ablowitz, J. Comput. Phys. **55,** 203 (1984).
20. Note that $1/\tau_N$ represents the decay rate into either of the ground states. However, the decay into $|2\rangle$ is 5/3 times more likely than the decay into $|1\rangle$ because of the degeneracy of these two ground states: $g_1 = 3$ and $g_2 = 5$. The decay time constants into the two states are given by $\tau_1 = \tau_N(g_1 + g_2)/g_1 = 43.5$ nsec and $\tau_2 = \tau_N(g_1 + g_2)/g_2 = 26.1$ nsec. We have ignored the effects; however, if τ_1 or τ_2 is used in place of τ_N, the saturation intensity will be somewhat lower.
21. H. M. Gibbs, S. L. McCall, and T. N. C. Venkatesan, Phys. Rev. Lett. **36,** 1135 (1976).
22. A. C. Tam and W. Happer, Phys. Rev. Lett. **38,** 278 (1977).